Combining Total Variation Regularization with Window-based Time Delay Estimation in Ultrasound Elastography

M. Mirzaei, A. Asif and H. Rivaz

This supplementary material contains more analysis on how the OVERWIND (tOtal Variation Regularization and WINDow-based time delay estimation) outperforms other methods of elastography. For the simulation result of Normalized Cross Correlation (NCC), we use different subsample displacement estimation methods as it is shown in Fig. 1. We also present a comprehensive comparison of NCC, GLUE and the OVERWIND methods by plotting all edge spread functions of target window for both simulated data and phantom experiments in Figs. 2-3. We also include results of Dynamic Programing and Analytic Minimization (DPAM) for all experiments. In addition to the phantom simulated in the main paper, we also present results on two additional phantoms, one with one inclusion and the other with two inclusions. We show axial strain images estimated with different methods on these new simulated phantoms.

It is worth noting that we have tuned both GLUE and OVERWIND methods very carefully and the presented strain fields in the paper are the best results of both methods. To further illustrate the behavior of two methods for different regularization weights, we show these results for one of the patients in Fig. 9. In this figure, the regularization weights are increasing from top to the bottom row. It is clear from these results that OVERWIND consistently outperforms GLUE for all regularization weights with three distinctive features: the strain image is sharper at the boundary of the tumor, it is smooth in uniform regions, and does not suffer from the two regions of low strain at the top and bottom of the images. These two regions provide more indication of biased results of GLUE, which systematically underestimates the strain.

I. Results

To perform subsample displacement estimates, we performed two different interpolation methods of cubic spline and 3-point parabolic interpolation. The results are shown in Fig. 1. It is important to note that similar to the NCC results in the main paper, the RF data here is upsampled by a factor of 10 in both axial and lateral directions using cubic spline interpolation. This interpolation is only performed for NCC and not for GLUE or OVERWIND. These results show that at such high sampling rates, the use of cubic spline or 3-point parabolic interpolation lead to very similar results as expected.

Figs. 2 and 3 plot the Edge Spread Function (ESF) for all horizontal and vertical lines within the target windows for simulation and phantom studies. As it is clear, OVERWIND has a smoother ESF than GLUE specially for high strain values.

Fig. 4 shows the results of DPAM for simulation, phantom and *in-vivo* data. As is clear from these results there is a discontinuity between strains of different RF lines because in DPAM the subpixel displacement of a RF line is calculated and it is used as an initial estimate for neighboring RF lines. Therefore, the main draw back of DPAM is that displacement estimates are discontinuous between adjacent RF-lines, which cannot be compensated by regularization. However, Kalman filter can be applied as an post-processing method to increase the smoothness between strain of neighboring RF lines as is shown in Fig. 5. It worth noting that the color range for the presented data are exactly same as the color range for other methods that are presented in the paper.

We have also simulated a phantom with a background Young's modulus of 4kPa, which has an inclusion with Young's modulus of 40kPa placed in the middle. Fig. 6 shows the performance of different methods in estimating the strain of this phantom. This figure demonstrate that OVERWIND outperforms other methods.

We simulated another phantom with a size of 32×32 mm^2 with two inclusions inside. The Young's modulus of phantom is 16 kPa and for the two inclusions, the Young's moduli are 40 and 70 kPa. The ground truth axial strain of the simulated phantom is shown in Fig. 7 (a). The results of GLUE and OVERWIND are shown in Fig. 7 (b) and (c). OVERWIND clearly outperforms GLUE in estimating the strain of the phantom and its inclusions. We show the lateral displacement estimated corresponding to this simulated phantom with the two inclusions in Fig. 8. It is clear from these images that the lateral displacement is substantially more accurate for OVERWIND especially in the regions pointed to by the black arrows.

Finally, we show results for one of the patients in Fig. 9 for different regularization weights. It is clear from these results that OVERWIND consistently outperforms GLUE in all regularization weights.

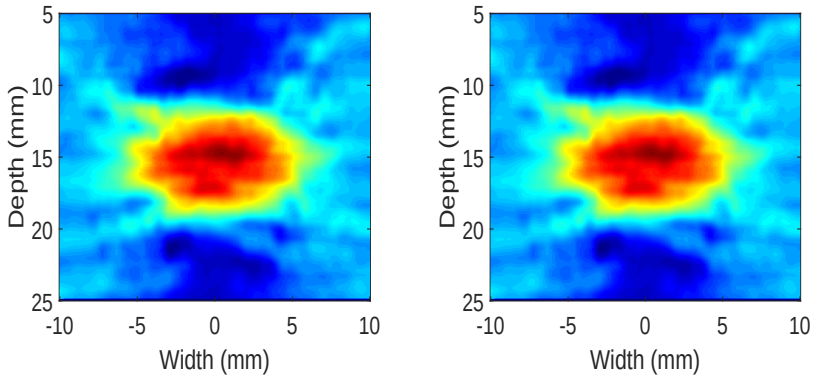

(a) (b)

Fig. 1: Strain of FEM simulated phantom with spline-based (a) and 3 point parabolic interpolations (b).

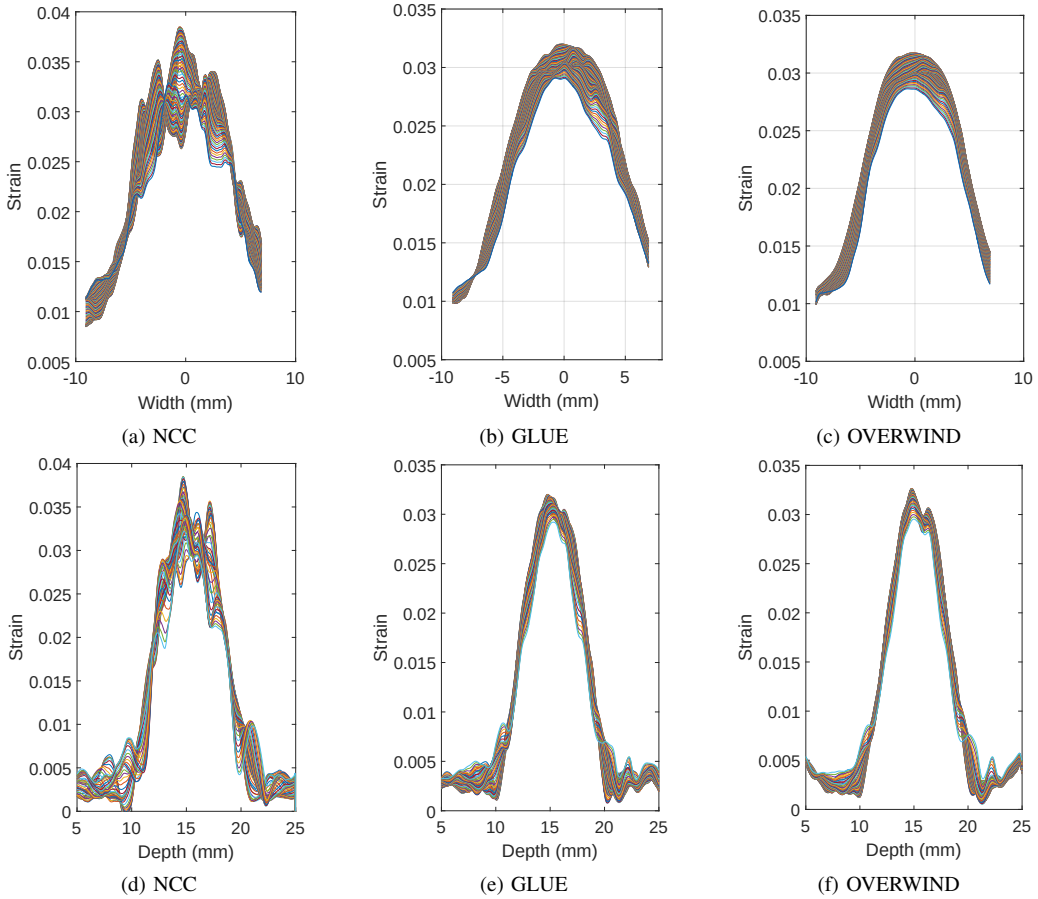

(a) NCC (b) GLUE (c) OVERWIND

(d) NCC (e) GLUE (f) OVERWIND

Fig. 2: ESF comparison for NCC, GLUE and OVERWIND for all points in the box for simulation data.

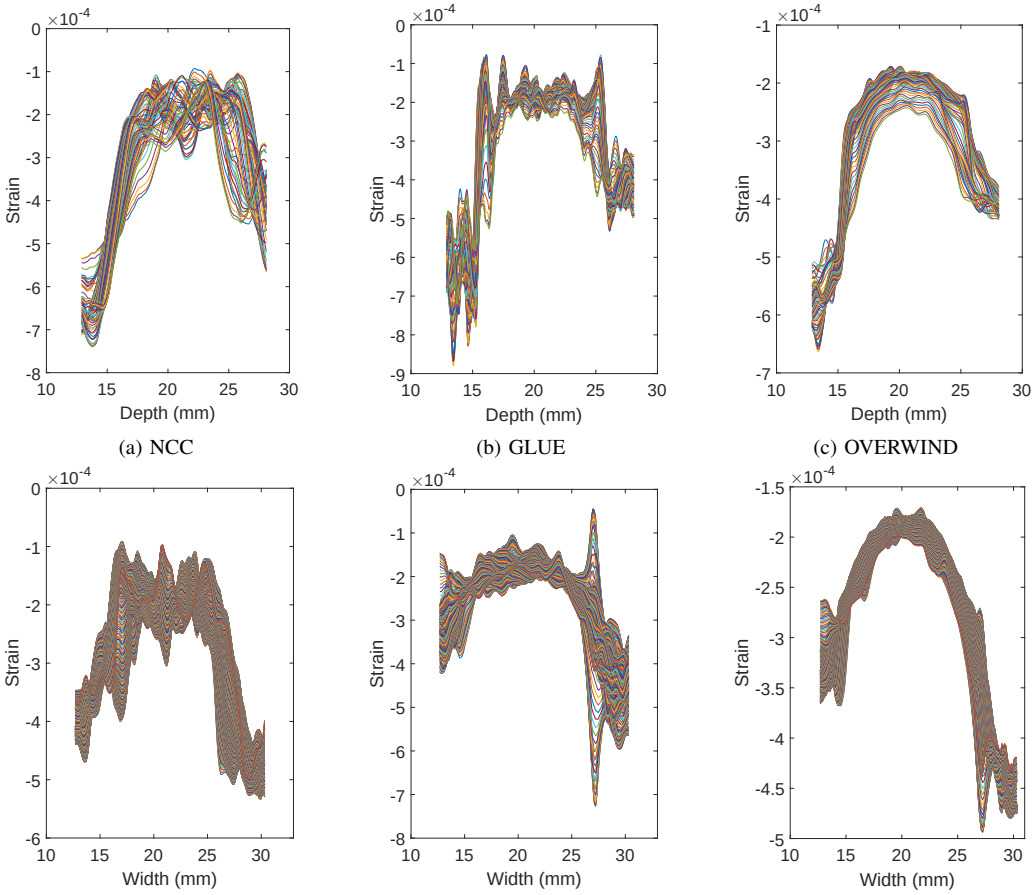

(a) NCC (b) GLUE (c) OVERWIND

(d) NCC (e) GLUE (f) OVERWIND

Fig. 3: ESF comparison for NCC, GLUE and OVERWIND for all points in the box for phantom data.

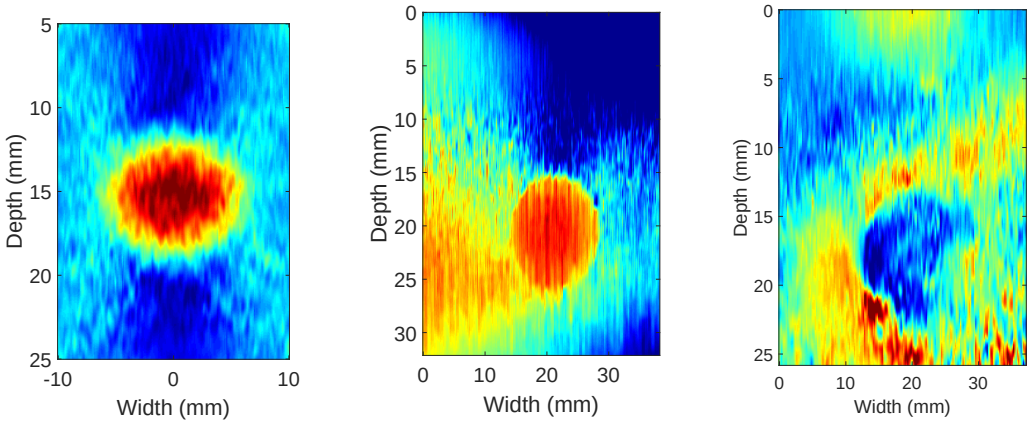

(a) Simulation (b) Phantom (c) Patient1

(d) Patient2 (e) Patient3

Fig. 4: Results of DPAM with LSQ

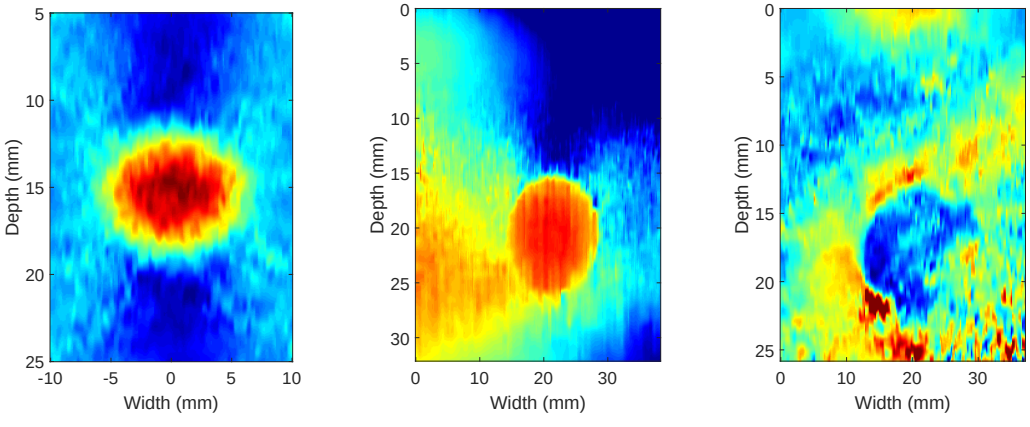

(a) Simulation (b) Phantom (c) Patient1

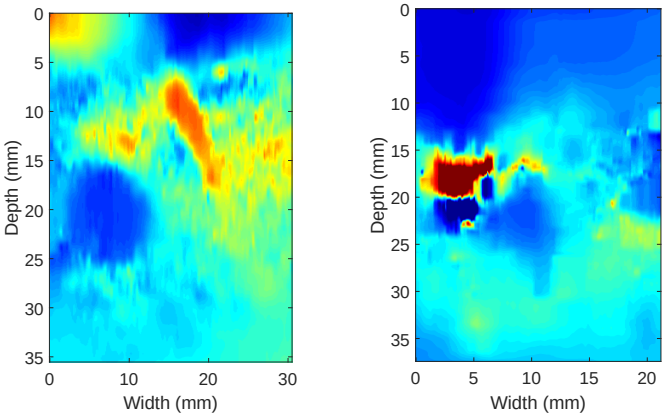

(d) Patient2 (e) Patient3

Fig. 5: Results of DPAM with Kalman LSQ

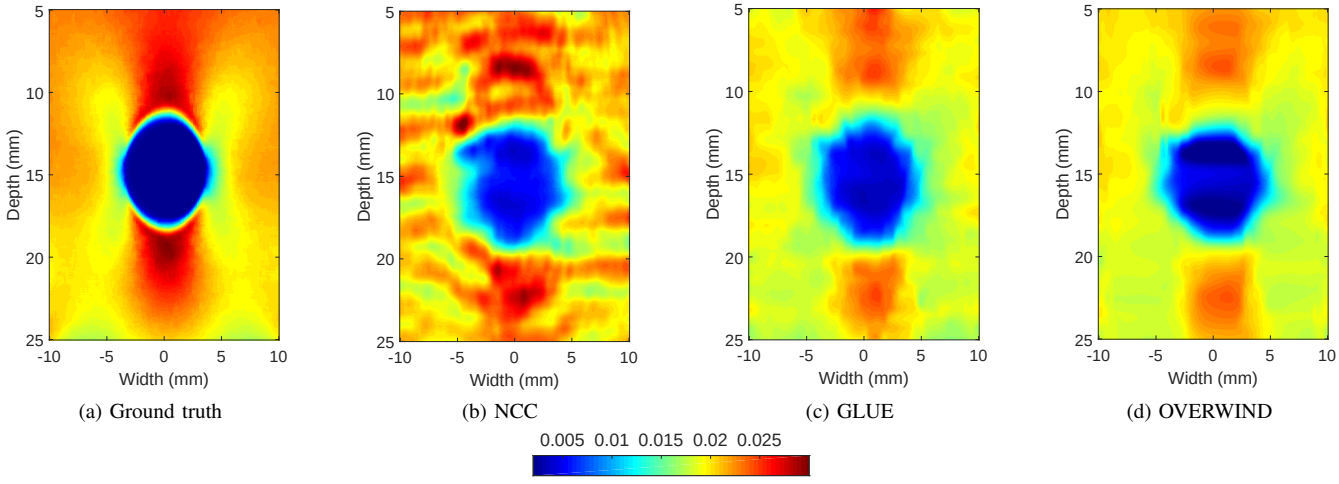

(a) Ground truth (b) NCC (c) GLUE (d) OVERWIND

Fig. 6: Strain estimated by three methods in the FEM simulated phantom.

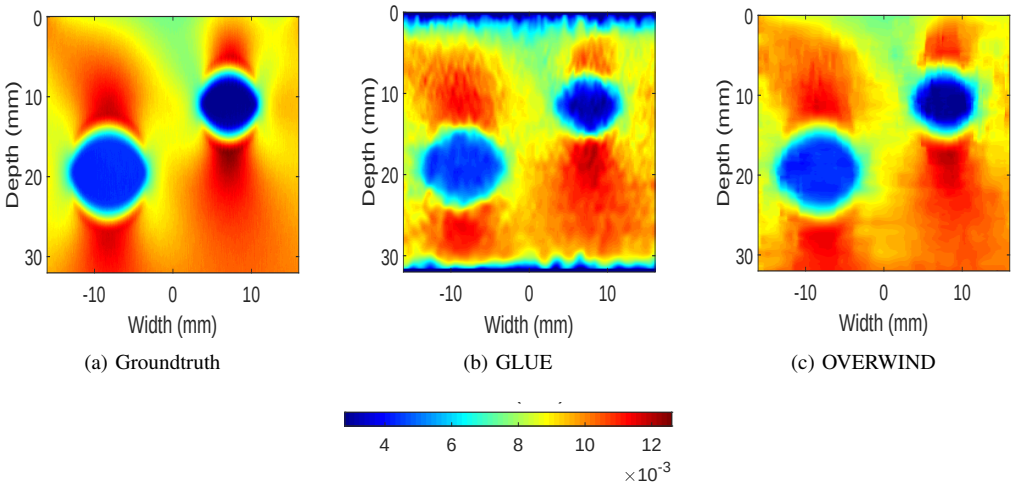

(a) Groundtruth (b) GLUE (c) OVERWIND

Fig. 7: Ground truth axial strain images for the FEM simulated phantom (a). Strain estimated by GLUE (b), and OVERWIND (c).

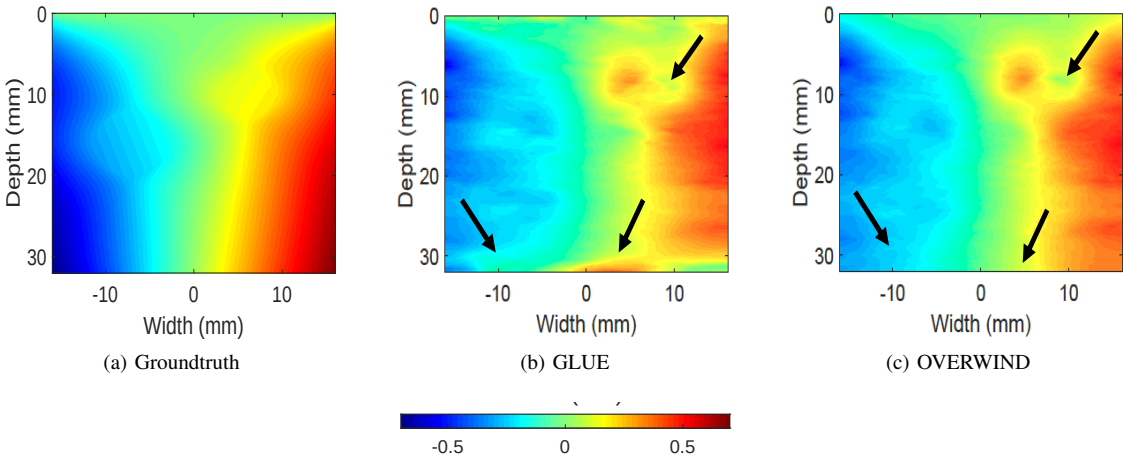

(a) Groundtruth (b) GLUE (c) OVERWIND

Fig. 8: Groundtruth of lateral displacement for FEM simulated phantom (a). The estimated lateral displacements with GLUE (b) and OVERWIND (c).

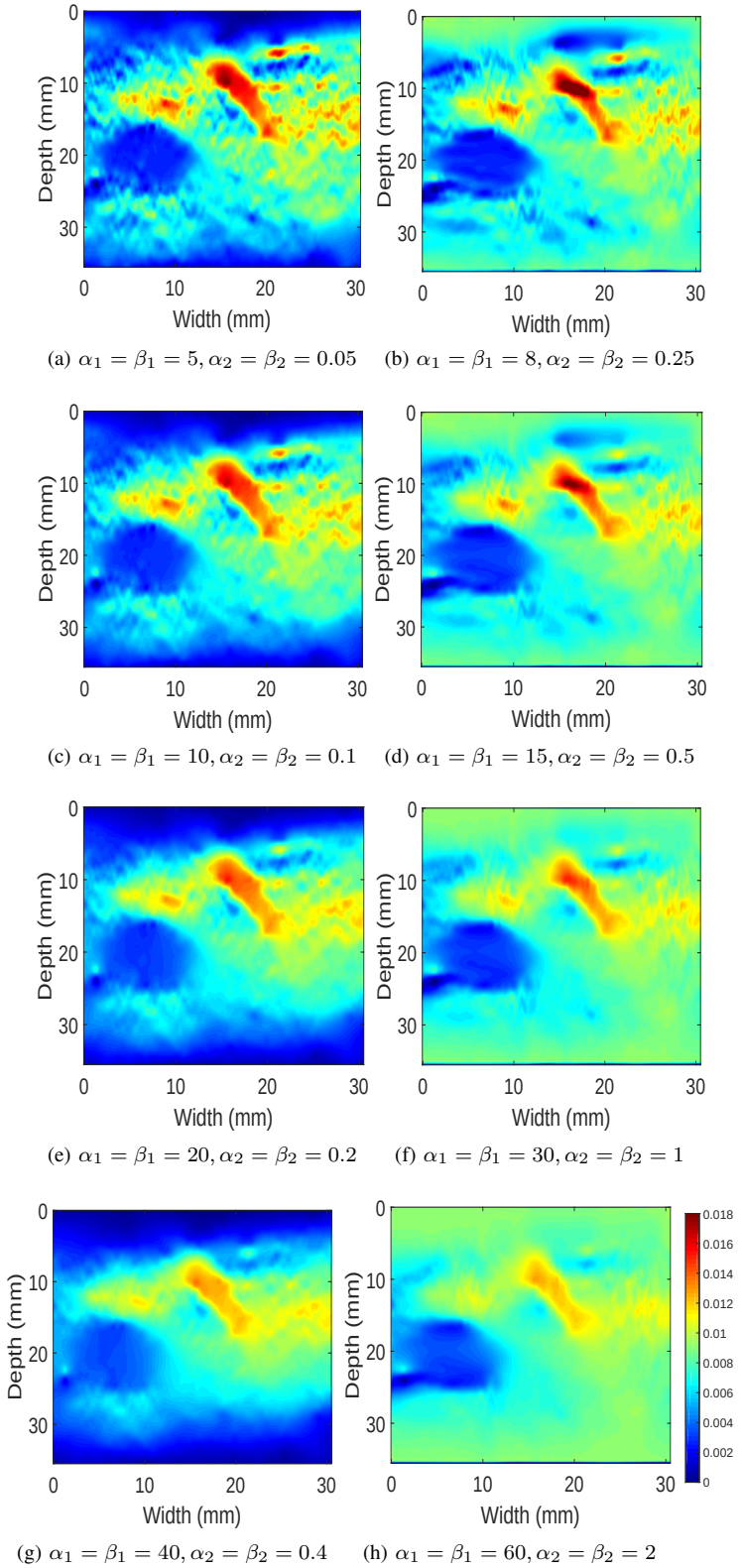

(a) $\alpha_1 = \beta_1 = 5, \alpha_2 = \beta_2 = 0.05$ (b) $\alpha_1 = \beta_1 = 8, \alpha_2 = \beta_2 = 0.25$

(c) $\alpha_1 = \beta_1 = 10, \alpha_2 = \beta_2 = 0.1$ (d) $\alpha_1 = \beta_1 = 15, \alpha_2 = \beta_2 = 0.5$

(e) $\alpha_1 = \beta_1 = 20, \alpha_2 = \beta_2 = 0.2$ (f) $\alpha_1 = \beta_1 = 30, \alpha_2 = \beta_2 = 1$

(g) $\alpha_1 = \beta_1 = 40, \alpha_2 = \beta_2 = 0.4$ (h) $\alpha_1 = \beta_1 = 60, \alpha_2 = \beta_2 = 2$

Fig. 9: Estimated strains by GLUE and OVERWIND with different regularization levels for one of the patients. The first column represents results of GLUE and the second column shows the results of OVERWIND.